Geosci. Model Dev. Discuss., https://doi.org/10.5194/gmd-2018-335
Manuscript under review for journal Geosci. Model Dev.
Discussion started: 20 March 2019

Geoscientific Model Development Discussions

CobWeb 1.0: Machine Learning Tool Box for Tomographic Imaging

Swarup Chauhan[1*], Kathleen Sell[1,3], Frieder Enzmann[1], Wolfram Rühaak[4], Thorsten Wille[5], Ingo Sass[2], Michael Kersten[1]

[1] Institute for Geosciences, Johannes Gutenberg-University, Mainz 55099, Germany
[2] Institute of Applied Geosciences, University of Technology, Darmstadt 64287, Germany
[3] igem – Institute for Geothermal Resource Management, Berlinstr. 107a, Bingen 55411, Germany
[4] Federal Institute for Geosciences and Natural Resources (BGR), Hannover 30655, Germany
[5] APS Antriebs-, Prüf- und Steuertechnik GmbH, Götzenbreite 12, Göttingen-Rosdorf 37124, Germany

Correspondence to: Swarup Chauhan (schauhan@uni-mainz.de)

Abstract.

Despite the availability of both commercial and open source software, an ideal tool for digital rock physics analysis for accurate automatic image analysis at ambient computational performance is difficult to pin point. More often image segmentation is driven manually where the performance remains limited to two phases. Discrepancies due to artefacts causes inaccuracies in image analysis. To overcome these problems, we have developed CobWeb 1.0 which is automated and explicitly tailored for accurate grayscale (multi-phase) image segmentation using unsupervised and supervised machine learning techniques. The simple and intuitive layout of the graphical user interface enables easy access to perform Image enhancement, Image segmentation and further to obtain the accuracy of different segmented classes. The graphical user interface enables not only processing of a full 3D digital rock dataset but also provides a quick and easy region-of-interest selection, where a representative elementary volume can be extracted and processed. The CobWeb software package covers image processing and machine learning libraries of MATLAB® used for image enhancement and image segmentation operations, which are compiled into series of windows executable binaries. Segmentation can be performed using unsupervised, supervised and ensemble classification tools. Additionally, based on the segmented phases, geometrical parameters such as pore size distribution, relative porosity trends and volume fraction can be calculated and visualized. The CobWeb software allows the export of data to various formats such as ParaView (.vtk), DSI Studio (.fib) for visualization and animation and Microsoft® Excel and MATLAB® for numerical calculation and simulations. The capability of this new software is verified using high-resolution synchrotron tomography datasets, as well as lab-based (cone-beam) X-ray micro-tomography datasets. Albeit the high spatial resolution (sub-micrometer), the synchrotron dataset contained edge enhancement artefacts which were eliminated using a novel dual filtering and dual segmentation procedure.

Geosci. Model Dev. Discuss., https://doi.org/10.5194/gmd-2018-335
Manuscript under review for journal Geosci. Model Dev.
Discussion started: 20 March 2019

1. Introduction

Currently a vast number of available commercial and open source software packages for pore-scale analysis and modelling exists (compiled in Figure 1), but dedicated approaches to verify the accuracy of the segmented phases are lacking. To the best of our knowledge, the current practice among researchers is to alternate between different available software tools and to synthesize the different datasets using individually aligned workflows. Porosity and in particular, permeability can vary dramatically with small changes in segmentation, as significant features on the pore-scale get lost when thresholding greyscale tomography images to binary images, even if using the most advanced data acquiring techniques like synchrotron tomography (Leu et al., 2014). Our new CobWeb 1.0 visualization and image analysis toolkit addresses some of the challenges of selecting representative elementary volume (REV) for X-ray computed tomography (XCT) datasets reported earlier by several researchers (Zhang et al., 2000; Gitman et al., 2006; Razavi et al., 2007; Al-Raoush and Papadopoulos, 2010; Costanza-Robinson et al., 2011; Leu et al., 2014). CobWeb 1.0 was customized to fill the gap by performing image analysis and accurate greyscale phase segmentation of reconstructed high-resolution XCT and synchrotron tomographic datasets. This software is based on a machine learning approach with great potential for segmentation analysis as introduced previously (Chauhan et al., 2016b; Chauhan et al., 2016a). Further, this software tool package was developed on a MATLAB® workbench and can be used as Windows stand-alone executable (.exe) files or as a MATLAB® plugin. Our hypothesis is that 3D tomographic REV analysis of Berea Sandstone™ (BS), Grosmont carbonate rock (GCR), and gas hydrate (GH)-bearing sediment datasets, would benefit of this new approach. Although the dataset for the latter GH geomaterials was acquired using monochromatic synchrotron X-ray, unhampered by beam hardening; Sell et al., (2016) highlighted problems with edge enhancement (ED) artefact and recommended image morphological strategies to tackle with this challenge. In this paper, we describe therefore also a strategy to eliminate ED artefacts using the same dataset but applying the new machine learning approach.

2. Materials and Methods

2.1. Gas-Hydrate bearing Sediment

The in-situ synchrotron-based tomography experiment and post-processing of synchrotron data conducted to resolve the microstructure of gas hydrate-bearing (GH) sediments is given in detail by Chaouachi et al. (2015), Falenty et al. (2015), and Sell et al. (2016). In brief, the tomographic scans were acquired with a monochromatic X-ray beam energy of 21.9 KeV at Swiss Light Source (SLS) synchrotron facility (Paul-Scherrer-Institute, Villigen, Switzerland) using the TOMCAT beamline (Tomographic Microscope and Coherent Radiology Experiment; Stampanoni et al. 2006). Each tomogram was reconstructed from sinograms by using the gridded Fourier transformation algorithm (Marone und Stampanoni 2012). Later, a 3D stack of 2560 x 2560 x 2160 voxels (volume pixels) was generated resulting in a voxel resolution of 0.74 µm and 0.38 µm at 10-fold and 20-fold optical magnification.

Geosci. Model Dev. Discuss., https://doi.org/10.5194/gmd-2018-335
Manuscript under review for journal Geosci. Model Dev.
Discussion started: 20 March 2019

2.2. Grosmont Carbonate Rock

The digital rock images of the Grosmont carbonate rock were obtained from the FTP server *GitHub* (http://github.com/cageo/Krzikalla-2012) used in the benchmark study published by Andrä et al., (2013a, 2013b). The Grosmont carbonate rock was acquired from Grosmont formation Alberta, Canada. The Grosmont formation was deposited during upper Devonian and is divided into four facies members, LG UG-1, UG-2, and UG-3 (bottom to top). The sample was taken from UG-2 facies and is mostly composed of dolomite and karst breccia (Machel and Hunter, 1994; Buschkuehle et al., 2007). Laboratory measurements of porosity and permeability reported by (Andrä et al., 2013b) are around 21 % ($\phi = 0.21$) and $\kappa = 150$ mD ─ 470 mD, respectively. The Grosmont carbonate dataset was measured at the high-resolution X-ray computer tomographic facility of the University of Texas with an Xradia MicroXCT-400 instrument (ZEISS, Jena, Germany). The measurement was performed using 4x objective lenses, 70 kV polychromatic X-ray beam energy, and a 25 mm CCD detector. The tomographic images were reconstructed from the sinograms using proprietary software and corrected for the beam hardening effect, which is typical for lab-based polychromatic cone-beam X-ray instruments (Jovanović et al., 2013). The retrieved image volume was cropped to a dimension of 1024^3 with voxel size of 2.02 µm

2.3. Berea Sandstone Rock

The Berea sandstone digital rock images were part of a benchmark project published by Andrä et al. (2013a, 2013b) and obtained from the *GitHub* FTP server. The Berea sandstone sample plug was acquired from Berea Sandstone Petroleum Cores ™ (Ohio USA). The porosity value of 20 % ($\phi = 0.20$) was obtained using a Helium pycnometer AccuPyc™ 1330 (Micromeritics Instrument Corp., Germany) and a Pascal-Mercury porosimeter (Thermo Scientific ™) as described in Giesche (2006). The permeability ranges between $\kappa = 200$ mD and $\kappa = 500$ mD as reported by Andrä et al. (2013b). Machel und Hunter (1994) identified minerals using a polarized optical microscope and a scanning electron microscope, and reported a mineral composition of Ankerite, Zircon, K-feldspar, Quartz, and Clay in the Berea sandstone sample. The synchrotron tomographic scans of Berea sandstone were also obtained at the SLS TOMCAT beamline. The beam energy was monochromatized to 26 keV for an optimal contrast with an exposure time of 500 ms. This resulted in a 3D tomographic stack with a dimension of 1024^3 voxels with a voxel size of 0.74 µm.

2.4. CobWeb Key Features

The first version of CobWeb offers the possibility to read and to process reconstructed XCT files in both .tiff and .raw formats. The graphical user interface (GUI) is embedded with visual inspection tools to zoom in/out, cropping, color, and scale, to assist in the visualization and interpretation of 2D and 3D stack data. Noise filters such as non-local means, anisotropic diffusion, median and contrast adjustments are implemented to increase the signal-to-noise ratio. The user has a choice of five different segmentation algorithms, namely K-means, Fuzzy C-means (unsupervised), least square support vector machine (LSSVM) (supervised), bragging and boosting (esamble classifiers) for accurate automatic segmentation and cross-validation. Relevant

material properties like relative porosities, pore size distribution trends, volume fraction (3D pore, matrix, mineral phases) can be quantified and visualized as graphical output. The data can be exported to different file formats such as Microsoft® Excel (.xlsx), MATLAB® (.mat), ParaView (.vkt) and DSI studio (.fib). The current version is supported for Micosoft® Windows PC operating systems (Windows 7 and 10).

The main GUI window panel divides into three main parts (Figure 2), the tool menu strip, the inspector panel, and the visualization panel. The tool strip contains menus for zoom in and out, pan, rotate, point selection, color bar, legend bar, and measurement scale functionalities. The inspector panel is divided into subpanels where the user can configure the initial process settings such as segmentation schemes (supervised, unsupervised, ensemble classifiers), filters (contrast, *non-local means*, *anisotropic* filter, *fspecial*), and distance functions (link distance, Manhattan distance, box distance) to assist segmentation and geometrical parameter selection for image analysis (REV, porosity, pore size distribution (PSD), volume fraction). The display subpanel *records*, displays the 2D video of the XCT stack and the respective histogram. History subpanel is a *uilistbox* that displays errors, processing time/status, processing instruction, files generated/exported and executed callbacks. Control subpanel is an assemblage of *uibuttons* to initialize the XCT data analysis process and the progress bar. Visualisation panel is where the results are displayed in several resized windows, which can be moved, saved or deleted. The pan-windows displayed inside the visualization module are embedded with *uimenu* and *submenu* to export, plot and calculate different variables like porosity, PSD, volume fraction, entropy, or receiver operational characteristics. To get the desired user functionalities, MATLAB® internal user-interface libraries where inadequate. Therefore, numerous specific adaptions are adopted from Yair Altman's undocumented Matlab website and the Matlab File Exchange community. Specifically, the GUI Layout Toolbox of David Sampson is used to configure the CobWeb GUI layout; the preprocessing *uitable*, uses the MATLAB java-component; it was designed using *uitable* customization report provided by (Altman, 2014).

As a stand-alone, the CobWeb GUI can be executed on different PC and HPC clusters without any license issues. The framework of CobWeb 1.0 is schematically illustrated in Figure 3 and the direction for the arrow (left to right) represents the series in which the various functions are executed. The backend architecture can be broadly classified in to three different categories, namely:

- Control module
- Analysis module
- Visualization module

2.4.1. Control module

Initially, the main figure panel is generated, followed by the tool strip dividing the main figure into different panels and subpanels as shown in Figure 2. After that, the control buttons *Load*, *Start*, *Stop*, *Volume Rendering* and *Clear* are created, initialized and the relevant information is appended in a main structure. Ideally, at this point, any button can be triggered or

activated. However, on doing so, an exception will be displayed in the history subpanel, indicating the next arbitrary steps. That is, to first load the data by pressing the *Load* button, where the *Load* function checks the file properties, loads the data in .tiff and .raw format, creates and displays 2D video of the selected stack, save the video file in the current folder, and updates the respective variables to the main structure. The *Stop* button (*Stop* function) ends the execution. However, when the processing is inside a loop, the *Stop* function can break the loop only after the i-th iteration. The *Clear* button (*Clear* function), deletes the data and clears all the variables in the main structure, resetting the graphical window.

2.4.2. Analysis module

The next step is data processing; triggered by pressing the *Start* button, which activates the *Start* function. The *Start* function concatenates the entire analysis procedure and is shown as Start () in Figure 3. It is a densely nested function, where the bullet points and the sub-bullet points shown in Figure 3, symbolizes the outer and the inner nested loops. Initially, the data is gathered and a sanity check is performed to evaluate, if the user, selected the relevant checkboxes and respective suboptions in the preprocessing *uitable*. If, the checkboxes are not selected, an exception alert is displayed in the *History* panel, highlighting the error and suggesting the next possible action. The next loop is the image modification loop, where the user inputs are required. These inputs are desired classes for segmentation, the image resolution, and the representative slice number. Thereafter, the representative slice is displayed on a resizable pan-window inside the visualization panel shown in Figure 2. Further, an option to select a region of interest (ROI) is proposed, which can be accepted or rejected. If accepted, a REV is cropped from the 3D image stack based on user defined ROI dimensions. On rejection, the complete 3D stack is prepared for processing.

The next step is the segmentation process; an unsupervised or supervised algorithm is initialized based on the selection made by the user in the preprocessing *uitable*. Hereafter, the programming logic implemented at the back-end for unsupervised and supervised segmentation schemes is briefly explained. It is an easy, one-step process in the case of unsupervised techniques. Based on the options selected in the preprocessing *uitable*, the image is filtered and subsequently, segmented. But, for unsupervised segmentation technique, Fuzzy C-means (FCM), an addition user input is required. A positive decimal number x, where x isequal to $1 \leq x \geq 2$ to set the membership criteria; when pixel values of different phases (ex. Rotligend sandstone, Gorsmont carbonate rock etc.) are in close vicinity or subsets of each other, FCM uses, the membership criteria to constain the segmentation 'loosely' or 'tightly' with the purpose to segregate different phases (Chauhan et al., 2016b).

In the case of supervised segmentation schemes (LSSVM, Bragging and Boosting) apriori information, also known as feature vector dataset or training dataset, is required to train the model(s) (Chauhan et al., 2016a; Chauhan et al., 2016b), and consequently, the trained model is ready to classify the rest of the dataset. The following five steps accomplish this procedure:

- First, the visualization panel displays a single 2D slice of the REV or 3D image stack in a resizable pan-window. The embedded *uimenu* in the pan-window offers to use the *subuimenu* opitons to feature vector selection, training and testing.
- Second, by pressing the *subuimenu* option *Pixel Selection*, the feature vector selection (FV) performs. The *Pixel Selection* callback function initializes the subroutine *uPixelSel()*, which sequentially displays a *uitable* in a resizeable

pan-window. The *uitable* contains columns *Features*, *X-Coordinate*, and *Y-Coordinate*, which is for example the pixel coordinates of pore, matrix, minerals, noise/speaks. This is a mandatory step, to build the training dataset. The user enters this information in the respective columns of the *uitable*.

- In the third step, the user has to identify features, such as, pores, minerals, matrix, noise/specks, in the 2D image, using zoom in and out tools available in the toolbar. The X-coordinates and Y-coordinates of the identified features need to be extracted using the data cursor tool, also available in the toolbar. If satisfied, the user can enter, the features and the corresponding X,Y coordinates in the *Pixel Selection uitable*.
- In the fourth step, the data is gathered and exported for training. This is done by pressing the export button placed on the *uitable* pan-window; which initiates the subrountine *uExportTable( )*. The export subroutine collects a total of 36 (6 x 6) pixel values in the perimeter of the user specified X,Y coordinates in the *uitable*.
- In the fifth step, the model is trained. This is done by using the *subuimenu* in the 2D pan-window. As and when the *training* is finished, a notification appears on the *History* panel. Thereafter by pressing the *testing* option in the *subuimenu* the complete REV or 3D stack can be segmented.

A progress bar offers to monitor the state of process. Further, the *History* window displays information related to processing time, implemented image filters and the segmentation scheme. Finally, all relevant information and the segmented data is append to the main structure.

2.4.3. Visualisation Module

Once the processing is finished, the segmented data can be visualized in 2D format using *Plot* button or in 3D rendered stack using *VolRender* button. Figure 3 depicts the nested loop structure of the *Plot ( )* and *VolRender ( )* callback functions. On initialization, the *Plot( )* callback accesses the main structure, and plots the segmented 2D image of the segmented slice consecutive, in a resizable pan-window in the visualization panel. The displayed pan-window is embedded with a *uimenu* and corresponding *subuimenu*. The *uimenu* items and the *subuimenu* options are

- Geometrical Parameters → Porosity, Pore Size Distribution, Volume Fraction
- Validation → Entropy, Receiver Operational Characteristics (ROC), 10-fold Cross Validation
- Export Stack → ParaView, Raw

The methods used to calculate geometrical parameters and validation schemes are benchmarked in (Chauhan et al., 2016a) (Chauhan et al., 2016b). Therefore, the selection of desired options initialize respective subroutines (uPoreSzVol, uCalVal, uExport) and plot the results as shown in Figure 2. If required, the export of these parameters (Porosity, PSD, Volume Fraction, Entropy, ROC; 10-fold Cross Validation) is possible to Excel, ASCII or MATLAB for further statistical analysis. Using the *Export Stack* item, the export of the 3D segmented volume to ParaView (.vtk files) or as .raw format files is feasible for the

purpose of visualization or DRP analysis. The volume rendering functionalities of CobWeb 1.0 is simple in comparison to ParaView or DSI studio. The *VolRender ( )* function renders the 3D data set using orthogonal plane 2-D texture mapping technique (Heckbert, 1986) and is best suited for OpenGL hardware. The user has the option to render the 3D stack in the original resolution or at lower resolution; the lower resolution enhances the plotting speed but degrades the image quality by 10-folds. Due to this, we recommend to export the 3D stack to ParaView or DSI studio for visualization.

3. Result and Discussions

3.1. Image Processing

Image pre-processing is one of the essential and precautionary steps before image segmentation (Iassonov Pavel et al., 2009; Schlüter Steffen et al., 2014). Image enhancement filtering techniques help to reduce artefacts such as blur, background intensity and contrast variation. Whereas, denoise filter such as median filter, non-local means filter, and anisotropic diffusion filter can assist in lowering the phase misclassification and improving the convergence rate of automatic segmentation schemes. CobWeb 1.0 is equipped with image enhancement and denoise filters, namely, *fspecial, imsharpen, non-local-means, anisotropic diffusion* which are commonly used in the XCT image analysis community. In total, 12 region of interest (ROIs) were investigated and suitable REVs were identified. Figure 4 shows the ROIs selected for the Berea, Grosmont and gas hydrate (GH) samples. In the case of Berea sandstone, the 3D reconstructed raw images (1024^3) had sufficient high resolution and contrast, thus did not show any noticeable change to the above mentioned filters. Whereas, the XCT images (1024^3) of the Grosmont carbonate rock needed a non-local means filtering which yielded in better visualization and performance results compared to those enhanced with anisotropic diffusion filter. However for GH synchrotron dataset, the CobWeb 1.0 filters were insufficient to normalize the edge enhancement artifact (ED), therefore a unique dual filtering scheme is implemented, which is explained in the following section 4.1.1.

3.1.1. Dual Filtering of Gas-Hydrate bearing Sediment

The ED artefact, is the high and low image contrast seen, between the edges, of the void, quartz and GH phases, in the GH tomograms. It certainly, aids in clear visual distinction, of these phases, but, becomes a nuisance during segmentation process. Several approaches to reduce ED artefact in GH tomograms and its effect on segmentation and numerical simulation have been discussed in (Sell et al., 2016). Based on our experience, a combination of the non-local means (NLM) filter and the anisotropic diffusion filter (AD), implemented using Avizo (ThermoFisher Scientific), works best in removing ED artefacts for our GH data. In short, AD was used for edge preservation and NLM for denoising.

3.1.1.1. Anisotropic Diffusion

For intuition purposes, Anisotropic Diffusion filter (AD) can be thought as (Gaussian) blur filter. AD blurs the image, where it carefully smooths the textures in the image by preserving its edges (Kaestner et al., 2008; Porter et al., 2010; Schlüter et al.,

Geosci. Model Dev. Discuss., https://doi.org/10.5194/gmd-2018-335
Manuscript under review for journal Geosci. Model Dev.
Discussion started: 20 March 2019

2014). To achieve the smoothing along edge preservation, the AD filter performs an iteration to solve non-linear partial differential equations (PDE) of diffusion:

$$\frac{\partial I}{\partial t} = c(x, y, t)\Delta I + \nabla c \,.\, \nabla I \qquad (1)$$

Where,

I is the image, t is the time of evolution and c is the flux which controls the rate of diffusion at any point in the image.

(P. Perona and J. Malik, 1990) introduce a flux function c to follow an image gradient and stop or restrain the diffusion when it reaches the region boundaries (edges preservation).

Given by

$$c(\|\nabla I\|) = e^{-(\|\nabla I\|\,\kappa)^2} \qquad (2)$$

$$(\|\nabla I\|) = \frac{1}{1+(\frac{\|\nabla I\|}{\kappa})^2} \qquad (3)$$

Here, the parameter κ is a tuning parameter that determines if the given edge to be considered as a boundary or not. Large value of κ lead to an isotropic solution and the edges are removed. For our investigations the parameter κ (threshold stop) was fixed to the value 22 968, which is the edge preservation limit between quartz grain and hydrate phase. The desired denoising (bluring/smoothing) was achieved within five iteration steps.

3.1.1.2. Nonlocal Means

Nonlocal means (NLM) filter is based on the assumption that the image contain an extensive amount of self-similarity (A. Buades et al., 2005; Shreyamsha Kumar, 2013). Based on this assumption Buades et al., (2005) extended the linear neighborhood SUSAN filter (Smith and Brady, 1997) with nonlocal class. Thus, through the nonlocal class, the spatial search for similar pixel values is not restricted to a constrained neighborhood pixel but the whole image is part of the search for similar pixel values. Given by the equation

$$NL(i) = \sum_{j \in I} w(i,j)v(j) \qquad (4)$$

Where,

$NL(i)$ is the estimated nonlocal intensity of the pixel *i*

I is the image

$w(i,j)$ is the weight (or average value) applied to noisy image $v(j)$ to obtain and restore the pixel *i.*

However, for practical and computational reason, the search is performed within a search window or neighborhood patches, and $w(i,j)$ evaluates similarity in pixel intensities between of local neighborhood patches. Where the weight $w(i,j)$ is calculated as

$$w(i,j) = \frac{1}{Z(i)}\, e^{-\frac{\left\|v(N_i)-v(N_j)\right\|^2_{2,\sigma}}{h^2}} \qquad (5)$$

Where. $Z(i)$ is a normalization constant

Geosci. Model Dev. Discuss., https://doi.org/10.5194/gmd-2018-335
Manuscript under review for journal Geosci. Model Dev.
Discussion started: 20 March 2019

$$Z(i) = \sum_j e^{-\frac{\left\|v(N_i)-v(N_j)\right\|^2_{2,\sigma}}{h^2}} \quad (6)$$

$v(N_i)$, $v(N_j)$ are the local neighborhood patches.

The similarity is fulfilled as the Euclidean distance between the local neighborhoods patches exponentially decreases.

$\sigma > 0$ is the standard deviation.

In eq. (5) and (6), the distance function $\left\|v(N_i) - v(N_j)\right\|^2$ is pointwise multiplied (convolved) with σ, to ensure fair contribution of pixel values to the weighted function. In this study, the NLM filter was set to a search window of 21, local neighbourhood of 6 and a similarity value of 0.71. The NLM filter was implemented in 3D mode to attain desired spatial and temporal accuracy and was processed on an CPU device.

3.2. Phase Segmentation

3.2.1. Grosmont Carbonate and Berea Sandstone Rock Samples

The K-means algorithm was used for the segmentation of REV analysis of Berea and Grosmont digital rock images. K-means is one of the simplest, yet,robust unsupervised machine learning (ML) algorithms commonly used in partitioning data (MacQueen, 1967; Jain, 2010; Chauhan et al., 2016b). Through an iterative approach the K-means algorithm computes the Euclidean distance between the data points (pixel value) to its nearest centroid (cluster). The iteration converges when the objective function, i.e. the mean square root error of Euclidean distance, reaches the minimum. This is, when each of the pixel in the dataset is assigned to its nearest centroid (cluster). However, the K-means algorithm has the tendency to converge at local minima without reaching the global minimum of the objective function. Therefore, it is recommended to repeatedly run the algorithm to increase the likelihood that the global minimum of the objective function will be identified. The performance of the K-means algorithm is influenced predominantly by the choice of the cluster centers (Chauhan et al., 2016b).

3.2.2. Gas Hydrate (GH) bearing Sediment Dual Clustering

The edge enhancement (ED) effect was significant in all the reconstructed slices of the GH dataset. The ED effect was noticeable around the quartz grains, with high and low pixel intensities adjacent to each other. The high intensity pixel values (EDH) were very close to GH pixel values, while the low intensity pixel values (EDL) showed a variance between noise and void phase pixel values. Therefore, immediate segmentation performed on the pre-filtered GH datasets using CobWeb 1.0 resulted in misclassification. Further parameterizing and tuning the unsupervised (K-means) and supervised (LSSVM) modules of CobWeb 1.0 specifically, distance function (i.e., functions euclidean distance *sqeuclidean*, sum of absolute differences *cityblock*, and *mandist*) and different permutation and combination between of kernel type, bandwidth and cross-validation parameters, showed significant improvement, but the segmentation was still not optimal. The aim was to eliminate the ED features completely without altering the phase distribution between GH and the void. This prompted to develop a GH-specific workflow as explained below. The appendix provides the MATLAB® script for this workflow comprised of 6 steps:

Step 1: Filtering and REV selection

Four REVs of size 4×700^3 were cropped from the raw (16 bit) data stack. These REVs were dual-filtered using AD and NLM filters (see section 4.1.1). Figure 5 depicts a 2D dual-filtered image from REV1.

Step 2: K-means clustering

After, dual-filtration (Step 1), it was essential to segregate the noise, edge enhancement effects and different phases into labels of various classes. This was accomplished by K-means segmentation. In order to capture all the phases accurately along with noise and ED effects a segmentation process with up to twenty class labels was needed and performed. As a result class seven captured all the desired phases (noise, edge enhancement low intensities (EDL), void, quartz, edge enhancement high intensities (EDH), GH).

Step 3: Indexing

In the next step the purpose was to retrieve pixel values of various phases from the dual-filtered REV stacks. The indexing scheme is the following:

- First, through visual inspection of the segmented image (step 2) different phases and their corresponding labels where identified, shown in Table 1.
- Thereafter, pixel indices of these phases, where extracted from the segmented image based on their labels.
- Further, these indices where used as a reference mask to retrieve pixel values of the phases from the 16-bit raw REV stacks.

The obtained pixel values represent noise, void (liquid), EDL, quartz, EDH, and GH phases in the raw images. Then, histogram distribution of the pixel values in each phase was plotted. The skewness of the histograms was investigated where the max, min, mean and standard deviation for each of the histogram was calculated. Thereafter, max and min of the histograms where compared, and the indexing limits were adjusted, for as-long-as there was no overlap found amidst the histogram boundaries.

Step 4: Rescaling raw REV

Now, in this step, the raw pixel values of the respective phases, i.e void, quartz, and GH, were replaced by their mean values, with an exception for EDH pixel values. The latter (EDH pixels) were replaced with the mean value of quartz. These assignments lead to optimal segregation of the phase boundaries in the raw dataset and finally to the elimination of the ED effect.

Step 5: K-means clustering

Geosci. Model Dev. Discuss., https://doi.org/10.5194/gmd-2018-335
Manuscript under review for journal Geosci. Model Dev.
Discussion started: 20 March 2019

Finally, the re-scaled raw REV was segmented into three class labels using K-means segmentation to obtain the final result.

3.3. Representative Elementary Volume

The REV is defined as the smallest volume, which should ideally represent the average effective macroscopic behavior of the geomaterial. Such that, the transport of the effective parameters (mass, momentum, energy) mathematically modelled within the REV becomes independent of the sample size (Wiącek and Molenda, 2016).

Figure 6 explains schematically the relationship between porosity and the volume of the porous media. In a small REV (region I), high fluctuation in porosity is contributed by the heterogeneity at the pore scale. As the volume increases (region II), and above a certain V_{min}, the porosity starts to normalize and iterates to a constant porosity value with small standard deviation. The porosity measured in this region is scale-independent, and is an accurate representation of a large-scale system. The increase in REV value above a V_{max} may result in increase/decrease in porosity in relationship to the heterogeneity, associated with `macroscopic' volume (region III) (Wiącek and Molenda, 2016). For heterogeneous porous media, porosity theoretically lies in-between region I and region III depending on the effective parameter under investigation; however, determination of ideal region II for real heterogeneous systems it may be difficult and subjective (Zhang D et al., 2000; Gitman et al., 2006; Razavi et al., 2007; Al-Raoush and Papadopoulos, 2010; Costanza-Robinson M.S. et al., 2011).

In particular, while performing permeability tensor simulation using XCT data, the size of minimum REV should be assessed not only based on porosity but also on geometrical parameters such as pore size distribution, void ratio, and coordinate number (Al-Raoush and Papadopoulos, 2010; Costanza-Robinson M.S. et al., 2011). For this study, we looked into different ROIs and their corresponding REV sizes between 300^3 to 700^3 voxels. Later, we established voxel size around 480^3 suited best for Berea and Grosmont and 700^3 voxels suited best for GH dataset. Figure 4 shows the chosen ROIs of Berea, Grossmont and GH dataset and Figure 7 and Figure 9 show the surface plot for respective REVs.

3.4. Estimation of Relative Porosity and Pore Size Distribution

In the case of the Grosmont carbonate and Berea sandstone, the respective REV's were segmented using K-means, as well as the PSD module based on the morphological scheme suggested in Rabbani et al. (2014) for the analysis. The mean relative porosity value of Berea sandstone is ϕ =17.3 ± 2.6 %, whereas for Grosmont carbonates the mean porosity value is lower (ϕ =10.5 ± 2.3 %) as shown in Figure 7. The regression coefficient value of R^2 = 0.092 for the Berea sandstone porosity trend indicates that porosity remains constant throughout the REV sizes chosen, and therefore consolidated for scale-independent heterogeneities. In the case of Grosmont carbonate rock, the chosen REV size was the best out of five obtained, which consolidate again for scale-independent heterogeneities. The average pore size distribution thus obtained was 6.70 µm ± 0.68 µm and 14.21 µm ± 0.66 µm for Berea and Grosmont plug samples, respectively.

Similarly, the porosity and PSD of the four GH REVs were analyzed using CobWeb 1.0 except but for image filtration and image segmentation, was performed using a different workflow as discussed in section 4.1.1 and 4.2.2. Figure 8 shows the

comparison of the porosity trends of different GH REVs. The low R^2 values of the porosity trends justify that, these GH REVs are scale-independent, and are an accurate representation of a large-scale system and are best suited for digital rock analysis. However, there is high variance compared with the mean PSD values. The exact reason is unknown, but may be due to the drastic increase and decrease of the quartz grains as can be noticed in Figure 5. The first and last 2D slices of ROI 1 in Figure 5 show either non-isotropic or isotropic distribution of quartz grains, which might have contributed to the respective high and low standard deviation seen in the porosity distribution. Figure 9 shows the surface and volume rendered plots of REV 1 and REV 2, due to the high accuracy of segmentation the quartz grain, brine and GH boundaries are clearly segregated and ED effect completely eliminated.

4. Conclusions and Outlook

This paper introduces with CobWeb 1.0 a new visualization and image analysis toolkit dedicated to representative elementary volume analysis of digital rocks. CobWeb 1.0 is developed on the MATLAB® framework and can be used as MATLAB® plugin or as a standalone executable. It offers robust image segmentation schemes based on machine learning (ML) techniques (unsupervised and supervised), were the accuracy of the segmentation schemes can be determined and results can be compared. Dedicated image processing filters such as the non-local means, anisotropic diffusion, averaging and the contrast enhancement functions help to reduce artefacts and increase the signal-to-noise ratio. The petrophysical and geometrical properties such as porosity, pore size distribution and volume fractions can be computed quickly on a single representative 2D slice or on a complete 3D stack. This had been validated using synchrotron datasets of the Berea sandstone (at a spatial resolution of 0.74 µm), a gas hydrate-bearing sediment (0.76 µm) and a high resolution lab-based cone-beam tomography dataset of the Grosmont Carbonate rock (2.02 µm). The gas hydrate dataset, despite its nanoscale resolution, was hampered with strong edge enhancement (ED) artefacts, which causes discrepancies in modelling and transport simulation. A combination of the dual filtering and dual clustering approach is proposed to completely eliminate the ED effect in the gas hydrate sediments, and the code is attached as an appendix. The REV studies performed on Berea sandstone, Grosmont carbonate rock and GH sediment using CobWeb1.0 shows relative porosity trends with very low linear regression values of 0.092, 0.1404, 0.0527 respectively. CobWeb1.0 ability to acurately segment data without compromise on the data quality at a resonable speed makes it an favorable tool for REV analysis.

CobWeb1.0 is still somewhat limited regarding its volume rendering capabilities, which will be one of the features to improve in the next version. The volume rendering algorithms implemented in CobWeb 1.0 so far do not reach the capabilities offered by ParaView or DSI studio, which relies on the OpenGL marching cube scheme. At present, the densely nested loop structure appears to be the best choice for systematic processing. As an outlook, vectorization and indexing approaches (*bsxfun*, *repmat*) have to be checked in detail to improve on processing speed. MATLAB®—Java synchronization will be explored further to configure issues related to multi-threading and visualization (Java OpenGL). Furthermore, a module CrackNet (crack network) is planned to be implemented, which will explicitly tackle the segmentation of cracks and fissures in geomaterials using

machine learning techniques and a mesh generation plugin (stl format) for 3D printing. Pore network extraction and skeletonization schemes such as modified maximum ball algorithm (Frederick Arand and Jürgen Hesser, 2017) and medial axis transformation (Katz and Pizer, 2003) will be considered such that the data can be exported to open-source pore network modelling packages (J. Gostick et al., 2016).

Code availability / Data availability

With regards to the code availability, the Matlab® code for removal of edge enhancement artifacts from the gas hydrate bearing sediment is attached as appendix. The CobWeb executable as well as the user manual and The gas-hydrate bearing sediment, XCT datasets are available to public on Zenodo repository http://dx.doi.org/10.5281/zenodo.2390943.

The CobWeb executable requires a Matlab runtime compiler R2017b (9.3), which can be downloaded and installed from https://ch.mathworks.com/products/compiler/matlab-runtime.html. The XCT dataset of Berea Sandstone and Grosmount Carbonate Rock can be obtained from *GitHub* FTP server (http://github.com/cageo/Krzikalla-2012). The gas-hydrate XCT datasets are not publicly available.

Author contribution

Contributor Roles Taxonomy (CrediT) is used to specify author contribution. https://casrai.org/credit/.

Swarup Chauhan conceptualized, investigated and performed the study. Further, implemented the machine learning workflow and graphical user interface design. Additionally, Swarup Chauhan performed the formal analysis and developed a software code for the removal of the edge enhancement artefact using the dual clustering approach. Further contributions of Swarup Chauhan: data curation on of the CobWeb software, writing the software manual, figures and writing, reviewing and editing the manuscript.

Kathleen Sell conceptualized, investigated and performed a case study on gas hydrates. Further, performed a study on the removal of edge enhancement artefacts and phase segmentation of methane hydrate X-ray tomograms (XCT). Also, she did a formal analysis by implementing dual filtration approach to reduce the edge enhancement artefacts. Kathleen Sell participated in discussions to validate phase segmentation using the dual segmentation approach and was involved in writing, reviewing and editing the manuscript

Frieder Enzmann was involved in the investigation of the X-ray tomography experiments and in acquiring synchrotron radiation beam time (TOMCAT beamline) at Paul Scherrer Institute, Villigen, Switzerland. He performed the reconstruction of XCT tomograms. Provided data curation in the form of archiving and maintenance - initial and later re-use for the XCT data.

Wolfram Rühaak was involved in the project administration of the CobWeb activities, provided resources with respect to graphical user interface (GUI) and inputs on improving GUI functionalities.

Thorsten Wille was involved in funding acquisition and sponsoring the CobWeb project, under the framework of the SUGAR (Submarine Gashydrat Ressourcen) III project by the Germany Federal Ministry of Education and Research grant number: 03SX38IH. He was involved in project administration and provided feedback on GUI functionalities

Ingo Sass was involved in the concept and funding acquisition for the CobWeb project, under the framework of the SUGAR (Submarine Gashydrat Ressourcen) III project by the Germany Federal Ministry of Education and Research (grant number: 03SX38IH) . He also provided supervision, project administration, resources and periodic review to improve GUI functionalities.

Michael Kersten was involved in conceptualization, preliminary investigation, funding acquisition for the project "Poroelastic wave propagation modelling on gas hydrate-bearing sediment based on tomographic microstructure data" from Deutsche Forschungsgemeinschaft (DFG grant number Ke 508/20 and Ku 920/18). He provided supervision, resources and was involved in writing, review and editing of the manuscript.

Acknowledgements

We thank Heiko Andrä and his team at Fraunhofer ITWM, Kaiserslautern, Germany, for providing us with the synchrotron tomography benchmark dataset of the Berea sandstone. The acquisition of the gas hydrate synchrotron-data was funded by the German Science Foundation (DFG grant Ke 508/20 and Ku 920/18). This study was funded within the framework of the SUGAR (Submarine Gashydrat Ressourcen) III project by the Germany Federal Ministry of Education and Research (BMBF grant 03SX38IH). The sole responsibility of the paper lies with the authors.

6. References

A. Buades, B. Coll, and J. M. Morel: A non-local algorithm for image denoising, in: 2005 IEEE Computer Society Conference on Computer Vision and Pattern Recognition (CVPR'05), 60-65 vol. 2, 2005.

Al-Raoush, R. and Papadopoulos, A.: Representative elementary volume analysis of porous media using X-ray computed tomography, Powder Technology, 200, 69–77, doi:10.1016/j.powtec.2010.02.011, 2010.

Altman, Y.: Accelerating MATLAB Performance, CRC Press, 2014.

Andrä, H., Combaret, N., Dvorkin, J., Glatt, E., Han, J., Kabel, M., Keehm, Y., Krzikalla, F., Lee, M., Madonna, C., Marsh, M., Mukerji, T., Saenger, E. H., Sain, R., Saxena, N., Ricker, S., Wiegmann, A., and Zhan, X.: Digital rock physics benchmarks—Part I: Imaging and segmentation, Benchmark problems, datasets and methodologies for the computational geosciences, 50, 25–32, doi:10.1016/j.cageo.2012.09.005, 2013a.

Andrä, H., Combaret, N., Dvorkin, J., Glatt, E., Han, J., Kabel, M., Keehm, Y., Krzikalla, F., Lee, M., Madonna, C., Marsh, M., Mukerji, T., Saenger, E. H., Sain, R., Saxena, N., Ricker, S., Wiegmann, A., and Zhan, X.: Digital rock physics

benchmarks—part II: Computing effective properties, Benchmark problems, datasets and methodologies for the computational geosciences, 50, 33–43, doi:10.1016/j.cageo.2012.09.008, 2013b.

Buschkuehle, B. E., Hein, F. J., and Grobe, M.: An Overview of the Geology of the Upper Devonian Grosmont Carbonate Bitumen Deposit, Northern Alberta, Canada, Natural Resources Research, 16, 3–15, doi:10.1007/s11053-007-9032-y, 2007.

Chauhan, S., Rühaak, W., Anbergen, H., Kabdenov, A., Freise, M., Wille, T., and Sass, I.: Phase segmentation of X-ray computer tomography rock images using machine learning techniques: an accuracy and performance study, Solid Earth, 7, 1125–1139, doi:10.5194/se-7-1125-2016, 2016a.

Chauhan, S., Rühaak, W., Khan, F., Enzmann, F., Mielke, P., Kersten, M., and Sass, I.: Processing of rock core microtomography images: Using seven different machine learning algorithms, Computers & Geosciences, 86, 120–128, doi:10.1016/j.cageo.2015.10.013, 2016b.

Costanza-Robinson M.S., Estabrook Benjamin D., and Fouhey David F.: Representative elementary volume estimation for porosity, moisture saturation, and air-water interfacial areas in unsaturated porous media: Data quality implications, Water Resour. Res., 47, doi:10.1029/2010WR009655, 2011.

Frederick Arand and Jürgen Hesser: Accurate and efficient maximal ball algorithm for pore network extraction, Comput. Geosci., 101, 28–37, doi:10.1016/j.cageo.2017.01.004, 2017.

Gitman, I. M., Gitman, M. B., and Askes, H.: Quantification of stochastically stable representative volumes for random heterogeneous materials, Archive of Applied Mechanics, 75, 79–92, doi:10.1007/s00419-005-0411-8, 2006.

Heckbert, P. S.: Survey of Texture Mapping, IEEE Computer Graphics and Applications, 6, 56–67, doi:10.1109/MCG.1986.276672, 1986.

Iassonov Pavel, Gebrenegus Thomas, and Tuller Markus: Segmentation of X-ray computed tomography images of porous materials: A crucial step for characterization and quantitative analysis of pore structures, Water Resour. Res., 45, doi:10.1029/2009WR008087, 2009.

J. Gostick, M. Aghighi, J. Hinebaugh, T. Tranter, M. A. Hoeh, H. Day, B. Spellacy, M. H. Sharqawy, A. Bazylak, A. Burns, W. Lehnert, and A. Putz: OpenPNM: A Pore Network Modeling Package, Computing in Science & Engineering, 18, 60–74, doi:10.1109/MCSE.2016.49, 2016.

Jain, A. K.: Data clustering: 50 years beyond K-means, Pattern Recognition Letters, 31, 651–666, doi:10.1016/j.patrec.2009.09.011, 2010.

Jovanović, Z., Khan, F., Enzmann, F., and Kersten, M.: Simultaneous segmentation and beam-hardening correction in computed microtomography of rock cores, Computers and Geosciences, 56, 142–150, doi:10.1016/j.cageo.2013.03.015, 2013.

Kaestner, A., Lehmann, E., and Stampanoni, M.: Imaging and image processing in porous media research, Quantitative links between porous media structures and flow behavior across scales, 31, 1174–1187, doi:10.1016/j.advwatres.2008.01.022, 2008.

Katz, R. A. and Pizer, S. M.: Untangling the Blum Medial Axis Transform, International Journal of Computer Vision, 55, 139–153, doi:10.1023/A:1026183017197, 2003.

Leu, L., Berg, S., Enzmann, F., Armstrong, R. T., and Kersten, M.: Fast X-ray Micro-Tomography of Multiphase Flow in Berea Sandstone: A Sensitivity Study on Image Processing, Transport in Porous Media, 105, 451–469, doi:10.1007/s11242-014-0378-4, 2014.

Machel, H. G. and Hunter, I. G.: Facies models for middle to late devonian Shallow-Marine carbonates, with comparisons to modern reefs: a guide for facies analysis, Facies, 30, 155–176, doi:10.1007/BF02536895, 1994.

MacQueen, J. (Ed.): Some methods for classification and analysis of multivariate observations, Fifth Berkeley Symposium on Mathematical Statistics and Probability, University of California Press, 281-297, 1967.

P. Perona and J. Malik: Scale-space and edge detection using anisotropic diffusion, IEEE Transactions on Pattern Analysis and Machine Intelligence, 12, 629–639, doi:10.1109/34.56205, 1990.

Porter, M. L. and Wildenschild, D.: Image analysis algorithms for estimating porous media multiphase flow variables from computed microtomography data: a validation study, Computational Geosciences, 14, 15–30, doi:10.1007/s10596-009-9130-5, 2010.

Porter Mark L., Wildenschild Dorthe, Grant Gavin, and Gerhard Jason I.: Measurement and prediction of the relationship between capillary pressure, saturation, and interfacial area in a NAPL-water-glass bead system, Water Resour. Res., 46, doi:10.1029/2009WR007786, 2010.

Razavi, M., Muhunthan, B., and Al Hattamleh, O.: Representative Elementary Volume Analysis of Sands Using X-Ray Computed Tomography, Geotechnical Testing Journal, 30, 212–219, doi:10.1520/GTJ100164, 2007.

Schlüter Steffen, Sheppard Adrian, Brown Kendra, and Wildenschild Dorthe: Image processing of multiphase images obtained via X-ray microtomography: A review, Water Resour. Res., 50, 3615–3639, doi:10.1002/2014WR015256, 2014.

Sell, K., Saenger, E. H., Falenty, A., Chaouachi, M., Haberthür, D., Enzmann, F., Kuhs, W. F., and Kersten, M.: On the path to the digital rock physics of gas hydrate-bearing sediments – processing of in situ synchrotron-tomography data, Solid Earth, 7, 1243–1258, doi:10.5194/se-7-1243-2016, 2016.

Shreyamsha Kumar, B. K.: Image denoising based on non-local means filter and its method noise thresholding, Signal, Image and Video Processing, 7, 1211–1227, doi:10.1007/s11760-012-0389-y, 2013.

Smith, S. M. and Brady, J. M.: SUSAN—A New Approach to Low Level Image Processing, International Journal of Computer Vision, 23, 45–78, doi:10.1023/A:1007963824710, 1997.

Wiącek, J. and Molenda, M.: Representative elementary volume analysis of polydisperse granular packings using discrete element method, Particuology, 27, 88–94, doi:10.1016/j.partic.2015.08.004, 2016.

Zhang D, Zhang R, Chen S, and Soll Wendy E.: Pore scale study of flow in porous media: Scale dependency, REV, and statistical REV, Geophys. Res. Lett., 27, 1195–1198, doi:10.1029/1999GL011101, 2000.

Geosci. Model Dev. Discuss., https://doi.org/10.5194/gmd-2018-335
Manuscript under review for journal Geosci. Model Dev.
Discussion started: 20 March 2019

Table 1: Class labels of different phases

Labels	**Phases**
0	Noise
1 and 3	Void (liquid)
2	Edge enhancement low intensities (EDL)
4	Quartz
5	Edge enhancement high intensities (EDL)
6 and 7	Gas hydrate

Geosci. Model Dev. Discuss., https://doi.org/10.5194/gmd-2018-335
Manuscript under review for journal Geosci. Model Dev.
Discussion started: 20 March 2019

Figures

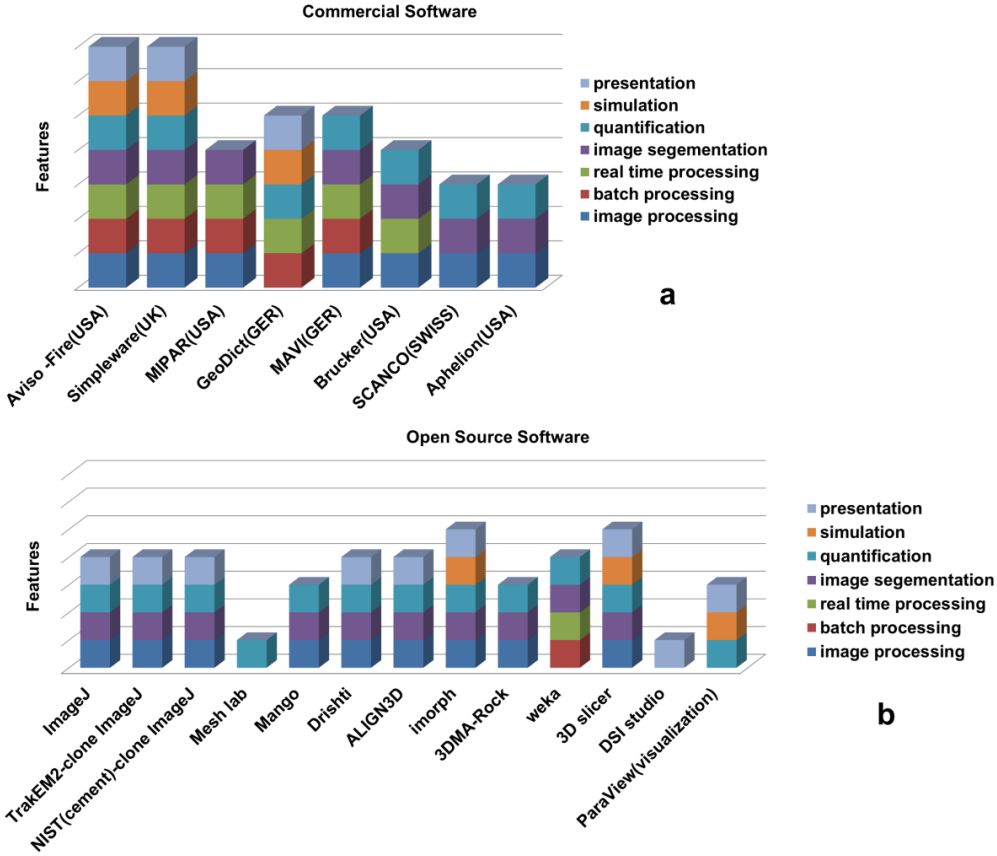

Figure 1: Market survey of the currently available commercial software (a) and open source software (b) assisting in digital rock physics analysis with features as indicated in legend

Geosci. Model Dev. Discuss., https://doi.org/10.5194/gmd-2018-335
Manuscript under review for journal Geosci. Model Dev.
Discussion started: 20 March 2019

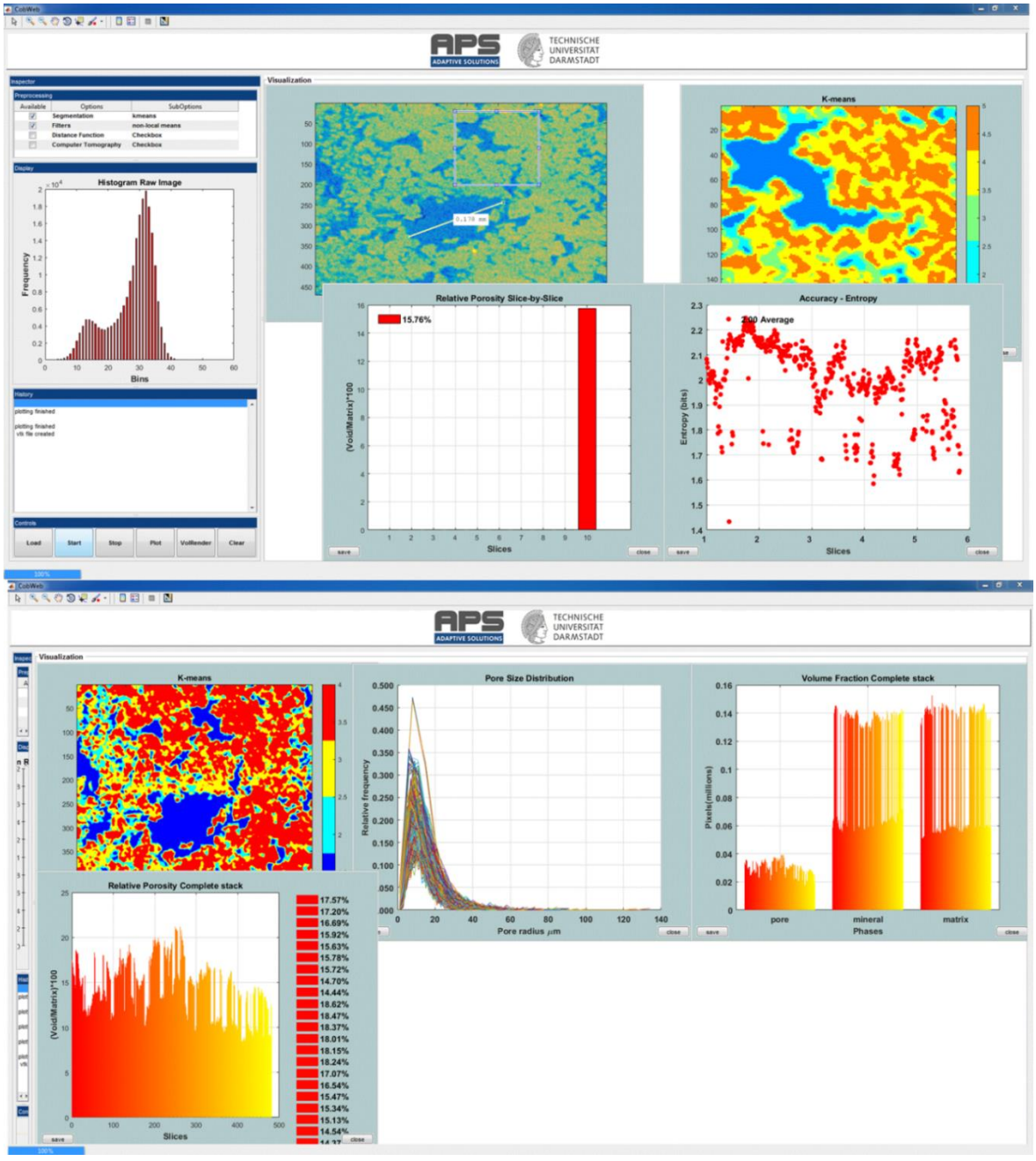

Figure 2: Snapshots of the CobWeb GUI. XCT stack of Grosmont Carbonate rock is shown as an example for representative elementary volume analysis. The top panel displays the XCT raw sample, the K-means segmented ROI, and the porosity of single slice No. 10. The bottom plot shows pore size distribution of the complete REV stack, the relative porosity and volume fraction, respectively

Geosci. Model Dev. Discuss., https://doi.org/10.5194/gmd-2018-335
Manuscript under review for journal Geosci. Model Dev.
Discussion started: 20 March 2019

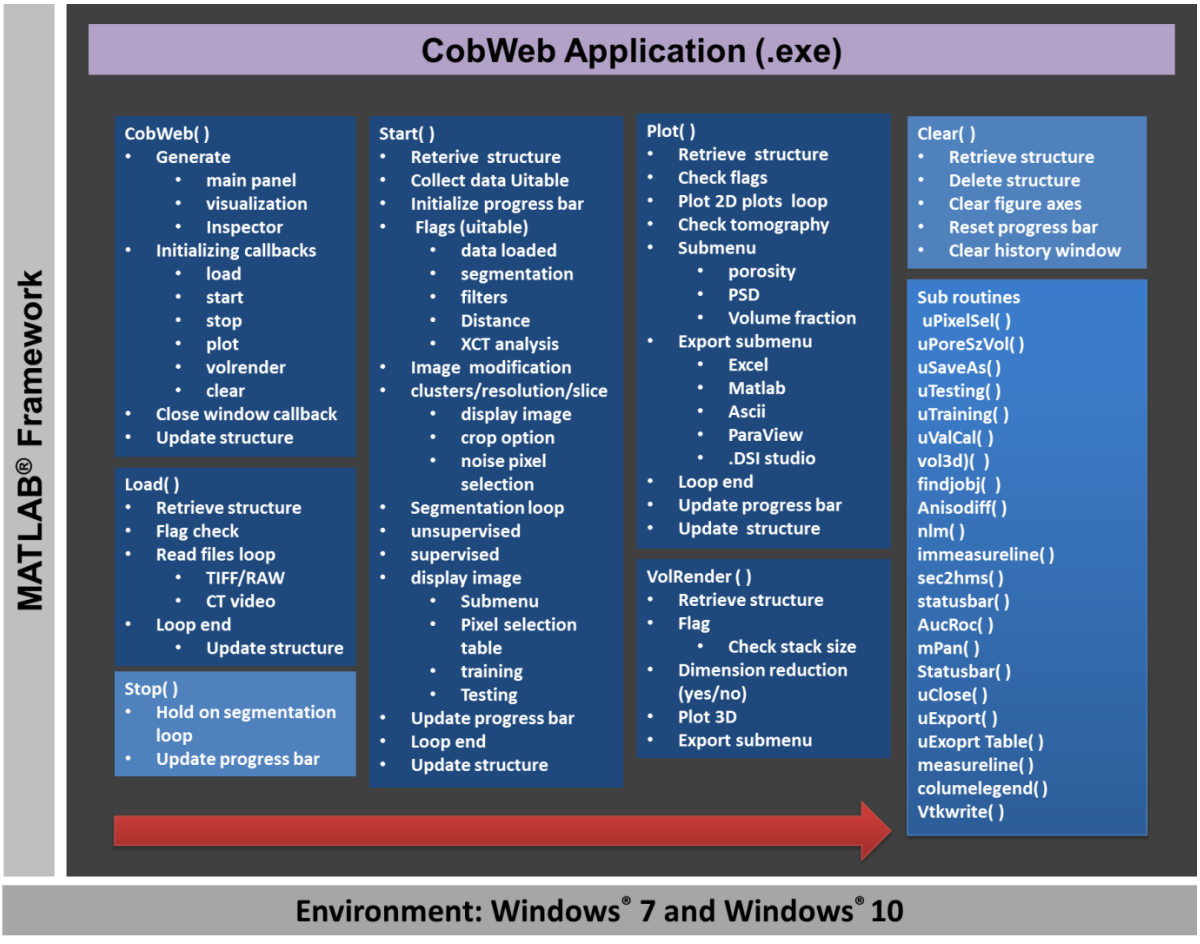

Figure 3: The general workflow of the CobWeb software tool, where the arrow denotes the series in which different modules are compiled and executed. A separate file script is used to generate .dll binaries and executables

Geosci. Model Dev. Discuss., https://doi.org/10.5194/gmd-2018-335
Manuscript under review for journal Geosci. Model Dev.
Discussion started: 20 March 2019

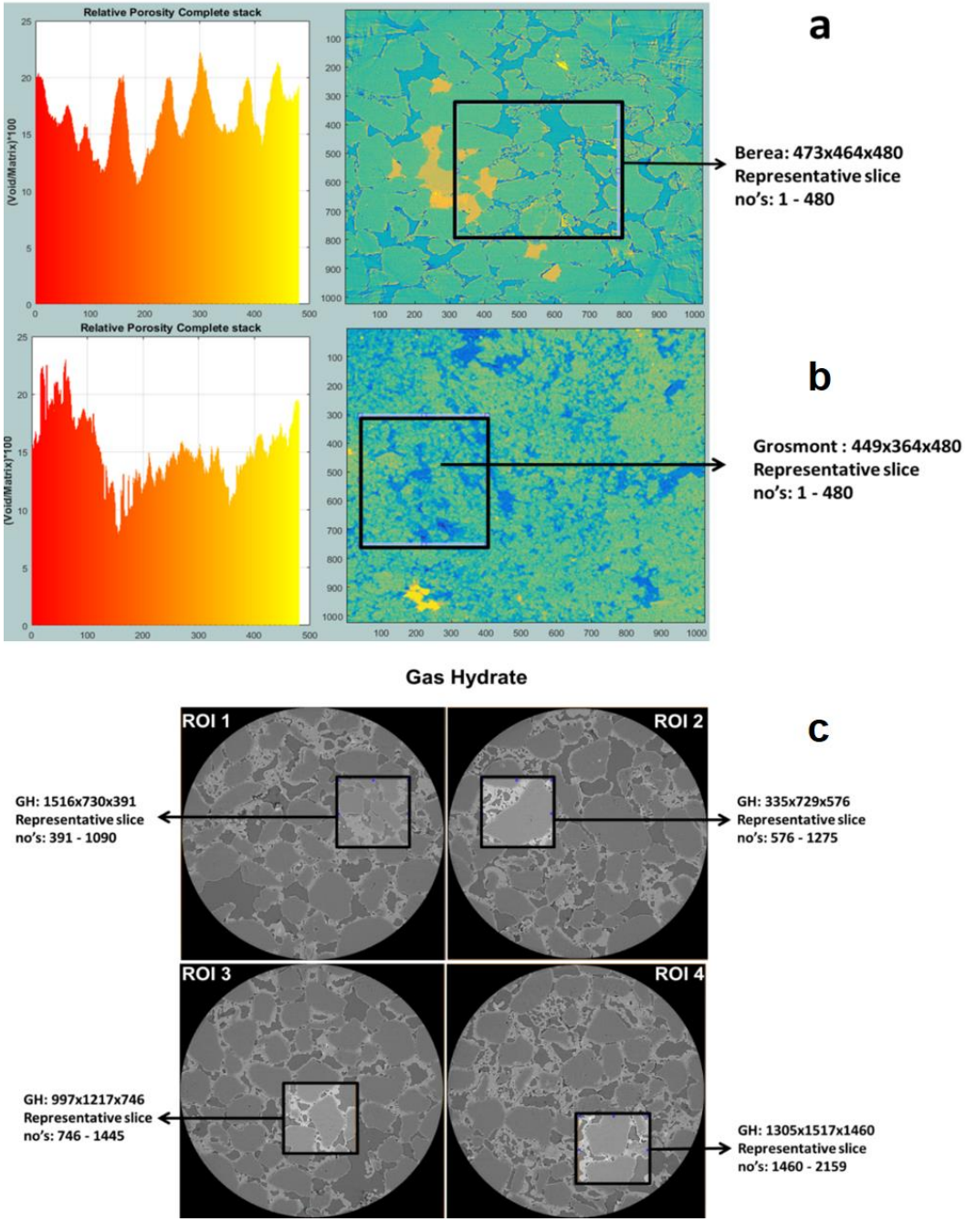

Figure 4: The most suitable ROIs and corresponding REV dimensions of Berea sandstone and Grosmont carbonate Gas Hydrate-bearing sediment is shown in the panel a b and c respectively

Geosci. Model Dev. Discuss., https://doi.org/10.5194/gmd-2018-335
Manuscript under review for journal Geosci. Model Dev.
Discussion started: 20 March 2019

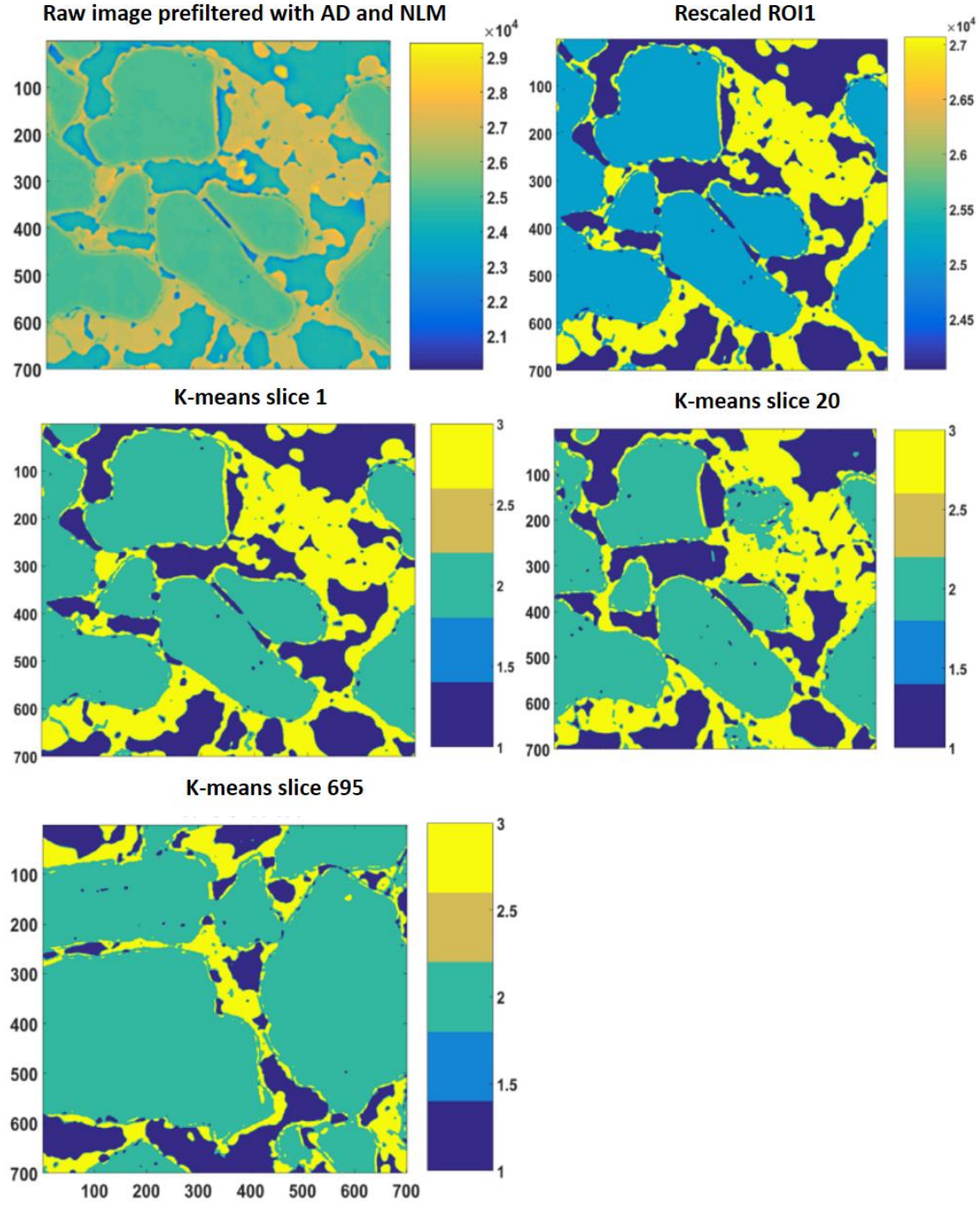

Figure 5: 2D filtered, rescaled, and segmented slices of gas hydrate REV1 dataset

Geosci. Model Dev. Discuss., https://doi.org/10.5194/gmd-2018-335
Manuscript under review for journal Geosci. Model Dev.
Discussion started: 20 March 2019

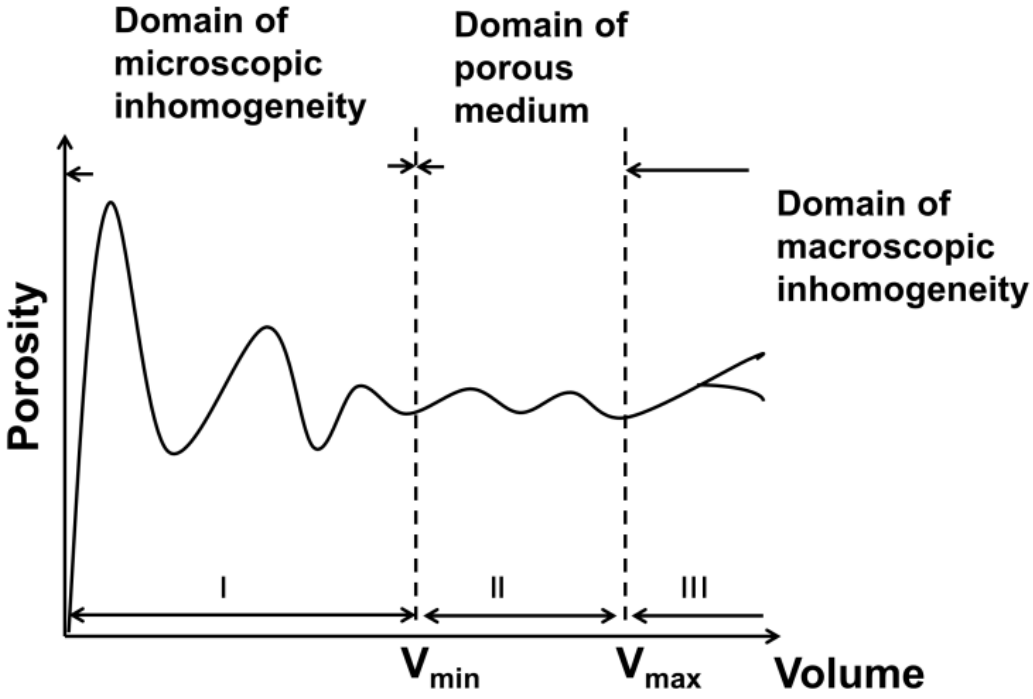

Figure 6: Schematic representation of the relationship between porosity (φ) and volume (V) of porous media. Bachmat and Bear (1986)

Geosci. Model Dev. Discuss., https://doi.org/10.5194/gmd-2018-335
Manuscript under review for journal Geosci. Model Dev.
Discussion started: 20 March 2019

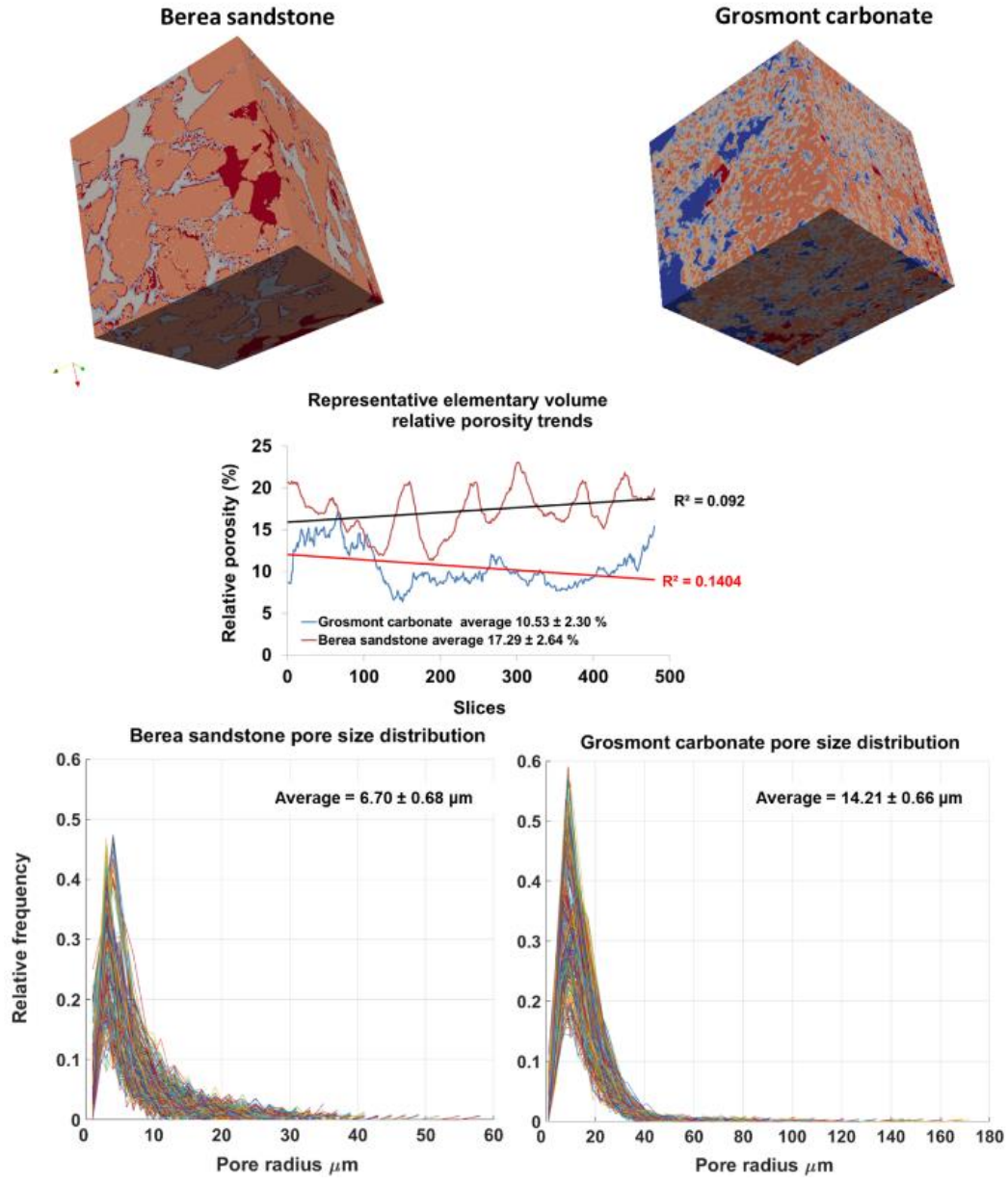

Figure 7: Top panel shows surface plot of REVs Berea sandstone and Grosmont carbonate (size 471x478x480) using visualisation software ParaView. Middle plot shows the relative porosity (%) trend for Berea sandstone and Grosmont carbonate REVs samples. Bottom plot shows the pore size distribution of Berea sandstone and Grosmont carbonate. XCT images were segmented using K-means. In the case of Grosmont, a non-local means filter was used

Geosci. Model Dev. Discuss., https://doi.org/10.5194/gmd-2018-335
Manuscript under review for journal Geosci. Model Dev.
Discussion started: 20 March 2019

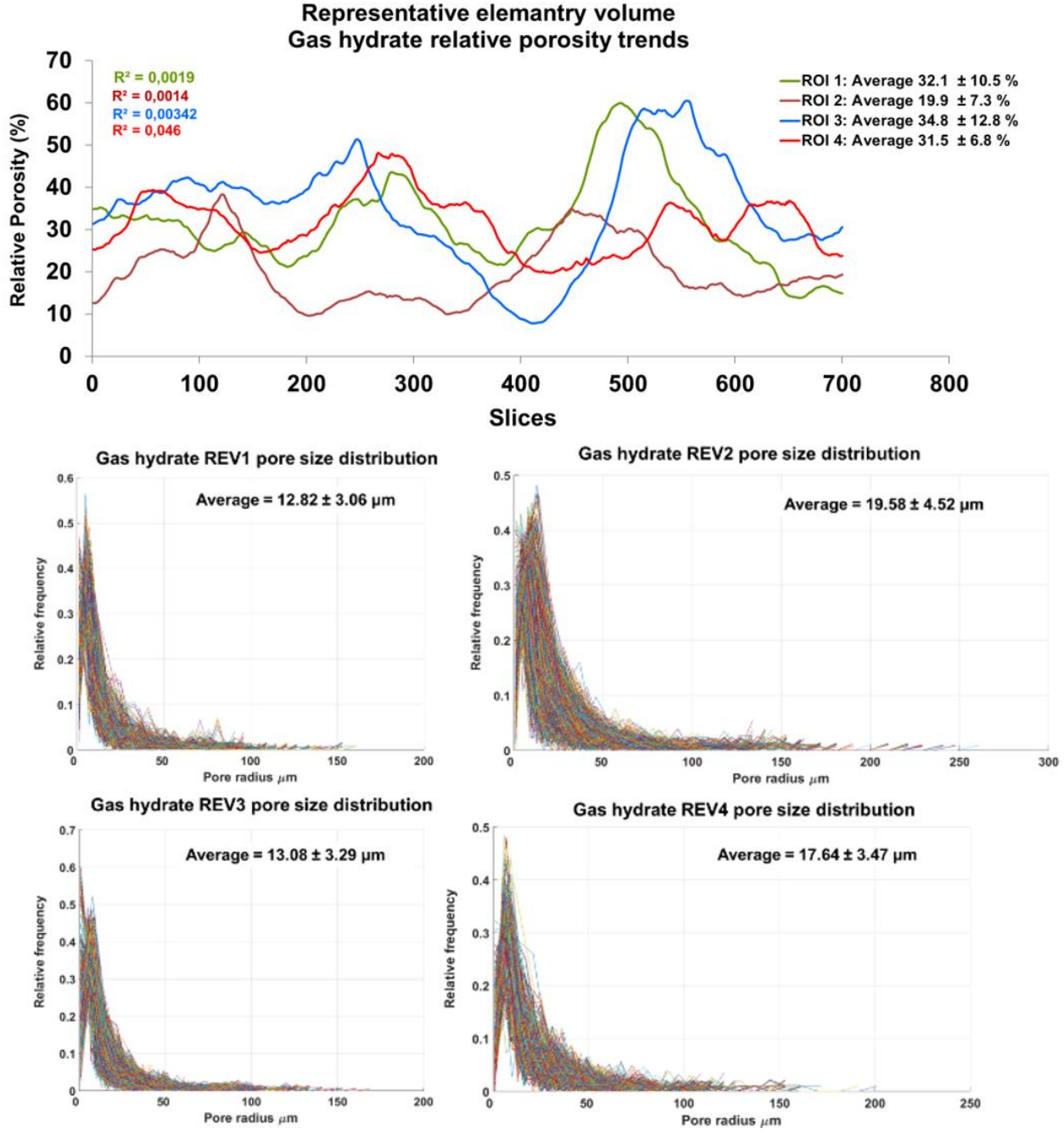

Figure 8: The top panel shows relative porosity trend analysis of gas hydrates, the middle and bottom panel show the geometrical pore size distribution of the respective REVs. The analysis was performed using CobWeb 1.0

Geosci. Model Dev. Discuss., https://doi.org/10.5194/gmd-2018-335
Manuscript under review for journal Geosci. Model Dev.
Discussion started: 20 March 2019

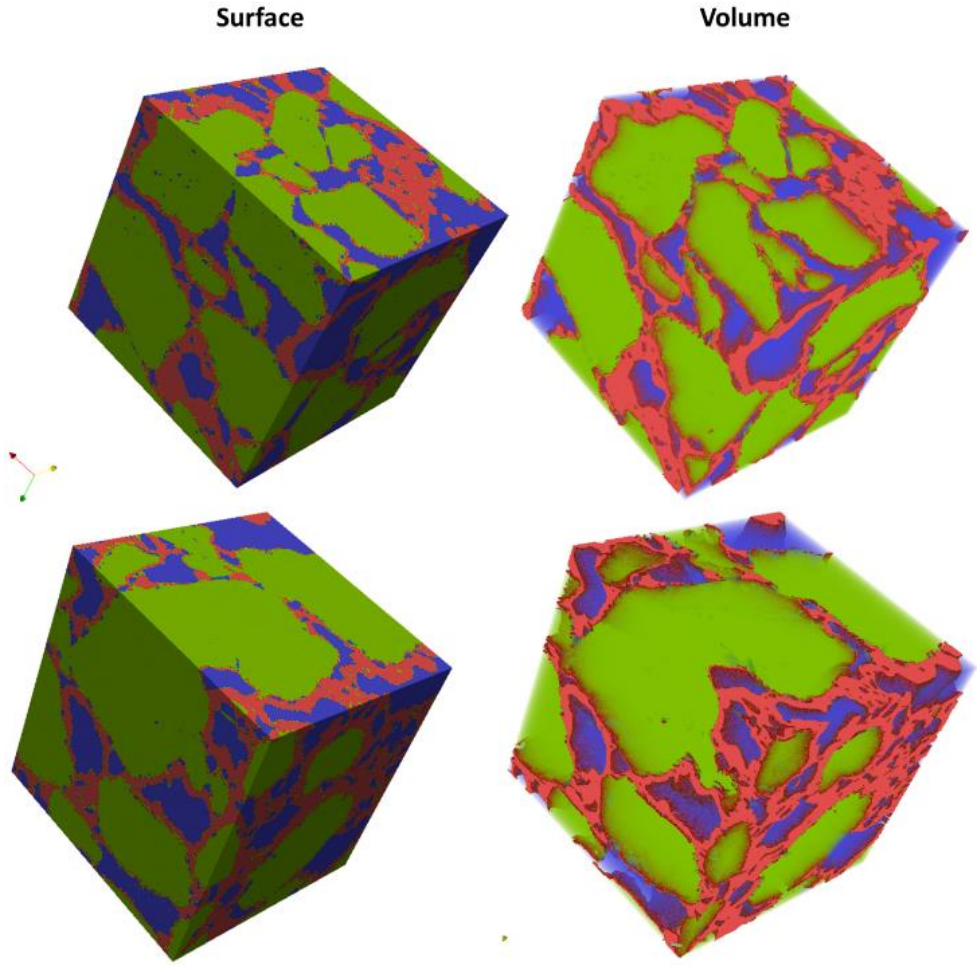

Figure 9: Segmented REVs of a gas hydrate sample displayed as surface and volume rendered. Analyzed using CobWeb 1.0 and exported to VTK format using CobWeb 1.0 ParaView plug-in. Quartz grain phase is represented in green color, gas hydrate in red, and in blue is the void space.